Adsorption of methylene blue onto betel nut husk-based activated carbon prepared by sodium hydroxide activation process

Mondira Bardhan, Tamanna Mamun Novera, Mumtahina Tabassum, Md. Azharul Islam, Ali H. Jawad and Md. Atikul Islam

ABSTRACT

In this study, activated carbon (AC) was prepared from agro-waste betel nut husks (BNH) through the chemical activation method. Different characterization techniques described the physicochemical nature of betel nut husks activated carbon (BNH-AC) through Fourier transform infrared spectroscopy (FTIR), Brunauer–Emmett–Teller (BET), scanning electron microscopy (SEM), and pH point of zero charge. Later, the produced AC was used for methylene blue (MB) adsorption via numerous batch experimental parameters: initial concentrations of MB dye (25–250 mg/L), contact time (0.5–24 hours) and initial pH (2–12). Dye adsorption isotherms were also assessed at three temperatures where the maximum adsorption capacity (381.6 mg/g) was found at 30 °C. The adsorption equilibrium data were best suited to the non-linear form of the Freundlich isotherm model. Additionally, non-linear pseudo-second-order kinetic model was better fitted with the experimental value as well. Steady motion of solute particles from the boundary layer to the BNH-AC's surface was the possible reaction dynamics concerning MB adsorption. Thermodynamic study revealed that the adsorption process was spontaneous and exothermic in nature. Saline water emerged as an efficient eluent for the desorption of adsorbed dye on AC. Therefore, the BNH-AC is a very promising and cost-effective adsorbent for MB dye treatment and has high adsorption capacity.

Key words | activated carbon, adsorption isotherm and kinetics, betel nut husks, desorption efficiency, dye removal, NaOH activation

Mondira Bardhan
Tamanna Mamun Novera
Mumtahina Tabassum
Md. Atikul Islam (corresponding author)
Environmental Science Discipline,
Khulna University,
Khulna 9208,
Bangladesh
E-mail: *atikku_es@yahoo.com*

Md. Azharul Islam
Forestry and Wood Technology Discipline,
Khulna University,
Khulna 9208,
Bangladesh

Ali H. Jawad
School of Chemistry and Environment, Faculty of Applied Sciences,
Universiti Teknologi MARA,
40450 Shah Alam, Selangor,
Malaysia

HIGHLIGHTS

- Betel nut husks activated carbon (BNH-AC) was prepared for the first time using sodium hydroxide (NaOH) activation with a 1:3 NaOH impregnation ratio.
- FTIR analysis of BNH-AC proved C=O and C–H functioned as active functional groups engaged in the reaction of cationic methylene blue (MB) dye.
- Adsorption of MB followed the Freundlich isotherm model and pseudo-second-order kinetics.
- The maximum adsorption capacities, qt (mg/g), were 381.6, 339.8 and 235.2 mg/g at 30, 40 and 50 °C.
- Negative ΔH°(kJ/mol) value indicated the adsorption process as exothermic in nature.

doi: 10.2166/wst.2020.451

GRAPHICAL ABSTRACT

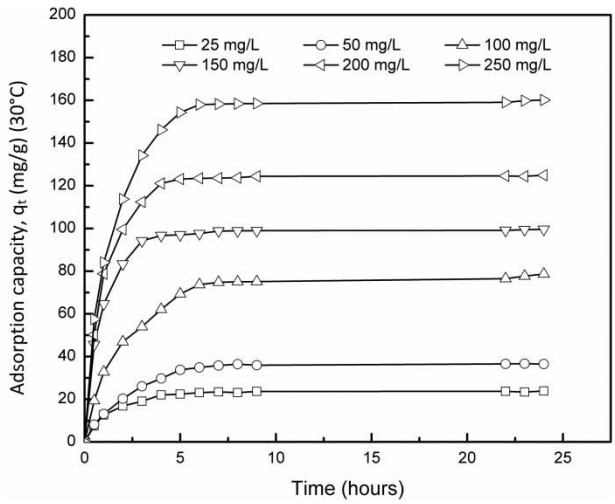

INTRODUCTION

Synthetic dyes, of which 800,000 tons are manufactured every year globally, are soluble in water, readily absorbed and are versatile colors in nature compared to natural dyes (Jamee & Siddique 2019). Despite having complex molecular structures and toxic characteristics, these dyes are increasingly used in chemicals, foods, textiles, paper, and the pharmaceutical industries, resulting in serious outcomes for human health and the environment (Islam *et al.* 2017a; Baumer *et al.* 2018). Like other developing countries, Bangladesh has undergone rapid industrialization, overpopulation and significant changes in the pattern of trade and finance industry for at least two decades (Shahbaz *et al.* 2014). Being the second largest garment-manufacturing nation in the world, this country dispenses a huge amount of dye effluent into its river system. Consequently, the overall quality of the receiving water is greatly damaged and has serious implications for human survival (Islam *et al.* 2011).

Methylene blue (MB), a cationic dye, is one of the most widely used dyes but one that causes eye burns in humans and animals, methemoglobinemia, cyanosis, convulsions, tachycardia, dyspnea, skin irritation and if ingested, irritation to the gastrointestinal tract, diarrhea and vomiting (Cazetta *et al.* 2011). When a river receives it, this results in immediate consequences, such as hindrance of sunlight to penetrate, damage done to various biological lifeforms, lowering the dissolved oxygen level, etc. The indirect impacts may involve eutrophication, acceleration of genotoxicity and microtoxicity (Khan & Malik 2014). Given the urgency to save the environment, certain methods such as precipitation (Cao *et al.* 2014), coagulation-flocculation (Kuppusamy *et al.* 2017), membrane filtration (Pereira *et al.* 2015) and adsorption (Ahmad *et al.* 2012; Kafshgari *et al.* 2017) have been implemented to remove dye. The adsorption method is considerably effective due to the feasibility and applicability of low-priced sorbents (Oyekanmi *et al.* 2019). It has great potential in significantly reducing such environmental problems, increasing productivity and helping to remediate the environment (Hoque & Clarke 2013). Several low-cost adsorbents, such as agricultural wastes, industrial solid wastes, biomass, clays minerals and zeolites, are usually utilized for MB removal (Rafatullah *et al.* 2010).

Activated carbon (AC) acts as an environmentally favorable and traditional adsorbent with a recognizable specific area, huge sorption capacity and various surface functional groups (Islam *et al.* 2017a; Kaykhaii *et al.* 2018). Nonetheless, the high manufacturing cost of AC impedes its widespread use (Rafatullah *et al.* 2010). In this context, native, inexpensive and available waste materials may be used to produce AC, which could help to advance the technology. Numerous studies have already been conducted to produce AC from waste fibrous biomass (flux) (Illingworth *et al.* 2019), palm bark (Melliti *et al.* 2020), pine cone, walnut shell, and

hazelnut shell (Kaya & Uzun 2020), sewage sludge (Chen *et al.* 2020), river sediment (Sang *et al.* 2019), *Butea monosperma* leaf (Das *et al.* 2020), palm kernel shell (Liew *et al.* 2018), rice straw (Sangon *et al.* 2018), *Artocarpus integer* peels (Selvaraju & Bakar 2017), waste biomass (Zubrik *et al.* 2017), coffee grounds (Rattanapan *et al.* 2017), oil palm waste (Rashidi & Yusup 2017), banana peels (Ingole *et al.* 2017), and many more. However, some biomasses are yet to be explored in terms of identifying their adsorption capacity when converted to AC material.

Betel nut (*Areca catechu*) is an evergreen, salinity-resistant tree and widely found in coastal areas of Bangladesh. Betel nut husks (BNH) comprise the unusable extraction and biodegradable fiber found in the betel nut fruits a chewing fruit of the Arecaceae family (Sultana *et al.* 2018). It is also grown in many tropical and sub-tropical areas like India, China, Indonesia, Malaysia, Myanmar and Nepal (Yusriah & Sapuan 2018). BNH comprise betel nut fruits, which contain around 60–80% of total volume and weight, and a single fruit generates approximately 2.50–2.75 g BNH (Hassan *et al.* 2010). It consists of α-cellulose, hemicellulose, lignin, pectin and proto-pectin, ash, and other materials of which the proportions of hemicellulose and lignin vary with its maturity (Hassan *et al.* 2010; Yusriah & Sapuan 2018). At the immature stage, both the husk and nut part are soft, where the outer layer of the fruit looks green (Yusriah *et al.* 2014). The juicier liquid husk becomes spongier when it ripens and the green color changes to brown and the fibers become coarser with maturation (Yusriah *et al.* 2014). With these physical and chemical properties, BNH are recognized as value-added products like composite materials, cushion, hardboards, and non-woven fabrics and housing insulation materials, although there are many unmanaged BNH which generate bad odor and landfill complications after harvesting (Borah & Dutta 2018). As a consequence, agro-waste like BNH requires better management with an emphasis on the waste-to-resource concept. Therefore, if pyrolysis of the BNH increases its adsorption capacity of MB, it will efficiently perform as a recycled product.

The adsorption capacities and textural properties along with its functional group of AC strongly depend on the mode of preparation, i.e. starting material, activation method, type of activator, and preparation conditions (Jawad *et al.* 2017; Rashid *et al.* 2018). AC can be generated by two activation methods: physical and chemical. Chemical activators can abate the activation temperature and time required compared to the physical activation method (Jawad *et al.* 2018). Both carbonization and activation are performed synchronously in this way in order to save cost and energy because low activation temperature is required to produce upgraded porous materials as well as high yield (Islam *et al.* 2017a; Jawad *et al.* 2018). NaOH is widely used as an effective chemical activator in preference to all other alkaline activating agents due to its availability and capacity to produce numerous pores on the AC's surface area (Heidarinejad *et al.* 2020).

There are many common natural feedstocks (especially, lignocellulosic materials) utilized as AC for removal of the cationic dye (MB). In the present study, we focused on inexpensive agro-waste: BNH. Dey *et al.* (2017) figured out the kinetic and isotherm characteristics of BNH over MB adsorption. However, for the first time, BNH, a native and very available agro-waste, was used to prepare BNH AC by using widely used effective chemical (NaOH) activation. Most importantly, the AC derived from BNH might attenuate the high production cost of commercial AC. The efficiency of obtained materials was assessed by how much MB was removed. Consequently, the main objective of this analysis was to produce a feasible and low-cost BNH-AC by NaOH activation that is also an environmentally friendly as well as economically viable adsorbent for the dispelling of model cationic MB dye. To compute the adsorption capacity, removal percentage, adsorption kinetics, isotherms, thermodynamics over MB solution as adsorbate were the major issues investigated here. To fit adsorption kinetic data, pseudo-first-order, pseudo-second-order kinetic models, intraparticle diffusion and film diffusion were determined. For analyzing the equilibrium data, the Langmuir and Freundlich isotherm models have been selected.

MATERIALS AND METHODS

Materials

BNH was collected from a local vendor (Gollamari, Khulna, Bangladesh) and washed to remove all undesirable materials. Then the moist BNH was dried in an oven at 105 °C until a constant weight was achieved. The dried BNH was ground in an electrical grinder to obtain the stock raw materials with a 2 mm particle size for BNH-AC preparation. MB dye, having a molecular weight 319.85 g/mol, chemical formula $C_{16}H_{18}ClN_3S.H_2O$, and solubility 40 g/L, was recognized as adsorbate and prepared 500 mg/L of stock solution. All chemicals used in this study were laboratory grade and commercially available.

Preparation of activated carbon

AC was obtained through pyrolysis and activation of raw BNH. The activation process was conducted by NaOH pellets (98% pure). Prepared BNH was mixed with powdered NaOH at three (1:1, 1:2 and 1:3) ratios (BNH:NaOH, w/w%) for 24 h at room temperature. The mixtures were then put into a crucible and placed into an air tight stainless-steel vertical tubular reactor. The temperature was 500 °C with a heating rate of 20 °C/min for 1 h. N_2 gas was simultaneously passed through the whole system with a constant flow rate. The reactor was allowed to cool at ambient temperature after ending its dwelling time. Then the activated chars were washed continuously utilizing deionized water till the pH of the products reached 6–7. The approximately neutral products were dried at 105 °C. After that, a preliminary study was carried out where the dye removal percentages were 56.93% (1:1), 62.08% (1:2) and 70.04% (1:3). So the 1:3 ratio was stored as stock absorbent since it had the highest removal percentage. This finalized product is referred to as BNH-AC.

Characterization of activated carbon

The Brunauer–Emmett–Teller (BET) surface area of BNH-AC was obtained from the N_2 adsorption-desorption isotherm at 77 K with a volumetric sorption analyzer (Micromeritics, Model ASAP 2060, USA). On the other hand, the surface morphology of the samples was observed through the scanning electron microscope (SEM) (Jeol, JSM-7610F). Surface organic structural groups on raw BNH and BNH-AC were studied by Fourier transform infrared (FTIR) spectra using Perkin–Elmer spectrometer (Model 2000, USA) in the 4,000–500 cm^{-1} range before and after adsorption of MB dye.

Determination of lignocellulosic and physical characteristics

The lignocellulosic content (cellulose, hemicellulose, lignin) was determined from extractive-free BNH. After proceeding with solvent extraction at 60 °C to determine the hemicellulose content, 1 g of extractive-free dried (at 110 °C) biomass was added to 150 mL of NaOH solution (20 g/L) and boiled for 3.5 h with distilled water. The residue was filtered, rinsed to remove Na, dried and finally weighted. The difference before and after treatment was the amount of hemicellulose. Lignin was calculated by the Klason method (Theander *et al.* 1995) where 15 mL of H_2SO_4 (72%) was added to 1 g of extractive-free dried biomass and heated for 2 h. The mixture was diluted up to 4% H_2SO_4 concentration and boiled for 4 h. Then the residue was filtered, washed, dried and weighted. The variation between before and after experiment revealed the lignin content. The amount of cellulose content was analyzed from the weight difference of extractives, hemicellulose and lignin.

A proximate analysis was carried out in both cases of raw BNH and BNH-AC. A measuring cylinder of 10 mL size was washed, dried and weighted. After filling the cylinder with both BNH and BNH-AC, it was further weighed. Likewise, for the determination of moisture content, at 105 °C, 1 g of both samples were oven dried for 24 h and weighed. The bulk density and moisture content of BNH and BNH-AC were calculated by using the following equations:

$$\text{Density } (gL^{-1}) = \frac{M_f - M_c}{V_c} \quad (1)$$

$$\text{Moisture content} = \frac{M_1 - M_2}{M_1} \times 100 \quad (2)$$

where, M_f demonstrates the weight of ground BNH and BNH-AC filled container and M_c is the weight of the container, and V_c is the volume of the container. M_1 and M_2 are the initial and oven-dried weight of the samples, respectively.

Ash content (%), volatile matter (%) and fixed carbon (% yield) of BNH and BNH-AC were obtained with a muffle furnace (HYSC, Model: MF -05, South Korea) and were calculated by following the mathematical expressions below:

$$\text{Ash content} = \frac{W_{ac} - W_c}{W_s} \times 100 \quad (3)$$

$$\text{Sample weight, } W_s = W_{rc} - W_{ac} \quad (4)$$

$$\text{Volatile matter} = \frac{W_{rc} - W_{ac}}{W_{rc}} \times 100 \quad (5)$$

$$\text{Fixed carbon} = [100 - (\text{ash content} + \text{volatile matter})] \quad (6)$$

where, W_c is the crucible weight (g), W_{rc} is the combined weight of crucible and samples (g): both BNH and BNH-AC, W_{ac} is the total weight of crucible and ash (g) that was determined after the experiment and W_s is the samples weight (g). Temperature was fixed at 550 °C for 4 h in case of determining the ash content, whereas analyzing the volatile matter was conducted at 900 °C for 7 min.

Batch adsorption performance

Batch adsorption mode experiments were conducted in 250 mL conical flasks with adsorbent dosage 0.20 g of BNH-AC and 200 mL of MB dye solution at six different concentrations (25, 50, 100, 150, 200 and 250 mg/L). The flasks were fixed in a thermostatic water bath shaker (GEM-MYCO, Model: YCW-012S, Taiwan), shaken at 150 rpm at 30, 40 and 50 °C, respectively. The common variables of interest such as solution pH (2–12), contact time (0–24 h), initial dye concentration (25–250 mg/L), and solution temperature (30–50 °C) were investigated to obtain equilibrium states for MB adsorption. The pH value of the dye solution was adjusted by adding H_2SO_4 (0.1 M) or NaOH (0.1 M) and monitored with a popular pH meter (HANNA, Model: pH 211, USA). At the fixed time intervals, the samples were picked up and a double beam UV–vis spectrophotometer (SHIMADZU, Model: UV – 1800, Japan) was used to determine the MB dye concentrations at λ_{max} 668 nm.

The amount of MB dye adsorbed by BNH-AC, q_e, (mg/g), kinetics q_t (mg/g) and removal percentage R (%) were calculated employing the following equations:

$$q_e = \frac{(C_0 - C_e)V}{W} \tag{7}$$

$$q_t = \frac{(C_0 - C_t)V}{W} \tag{8}$$

$$R(\%) = \frac{(C_0 - C_e)}{C_0} \times 100 \tag{9}$$

where C_0 is the initial MB concentration (mg/L), C_e and C_t are the concentration of MB (mg/L) at the equilibrium and time t, respectively, V is the volume of MB solution (L), and W is the mass of BNH-AC (g). By carrying out the fit of the experimental values to the non-linear equations, all the kinetics and isotherms models were analyzed using a scientific data analysis.

The pH point of zero charge (pH_{pzc}) was carried out by pH drift method. Patawat *et al.* (2020) recently determined the pH_{pzc} of AC derived from *Dipterocarpus alatus* fruit by adopting this method. The pH of a series of 0.01 M NaCl was adjusted at a different initial pH value ranging from 2 to 12; 0.1 M H_2SO_4 and 0.1 M NaOH were used for the adjustment. Then, 0.20 g of BNH-AC was added to each adjusted solution (50 mL). The dispersions were shaken for 48 h at 40 °C like the above stated procedure for pH, and the final pH of the solutions (pH_f) was determined by a pH meter. The pH_{pzc} is the point where the curve pH_f vs. pH_i intersects the line $pH_f = pH_i$. Its main purpose is to identify the anionic or cationic surface charge of the adsorbent.

Sorption isotherms and kinetics

The relationship between the amount of MB adsorbed over per unit mass of the sorbent and the different concentrations of dye stuff can be resolved by isotherm analysis. Along with this, it is easy to understand the adsorption performance of BNH-AC and adsorption dynamics of MB with time. Likewise, the kinetic studies can work out the kinetic mechanisms of the adsorption process. Both studies were carried out to assess the equilibrium experimental parameter states in the context of the maximum removal of dye. Batch adsorption experiments were done in 250 mL Erlenmeyer flasks holding 200 mL of MB solution (concentrations: 25 to 250 mg/L). The pH of the solutions was 6.4, close to the neutral value. Then, 0.2 g of adsorbent material (BNH-AC) was added to the flasks, which were placed in a temperature controlled horizontal shaker with agitating speed of 150 rpm. The temperature was 40 °C and after reaching the equilibrium time, the samples were extracted from the flasks and supernatant solutions were measured by using double beam UV–vis spectrophotometer at a wavelength of 668 nm. The amount of the uptake of MB by BNH-AC at optimum time was found by mathematical Equation (7). From the experimental data, the adsorption mechanism was recognized by two diffusion models: intraparticle and film. Moreover, a thermodynamic study was conducted using the same procedure beyond the temperature ranges of 30 °C to 50 °C. It is, basically, used to determine the effect of temperature on the nature and suitability of MB adsorption onto BNH-AC.

RESULTS AND DISCUSSION

Physical and chemical characteristics of adsorbent

The ratio of lignin, cellulose and hemicellulose of raw BNH and physical constituents of both BNH and BNH-AC are computed in Table 1. Bulk density of raw material was 0.245 g/mL. Table 1 reveals the compositional properties of BNH, including the maximum ratio of cellulose (46%), which is virtually identical to a previous study of areca nut husk (Chandra *et al.* 2016). AC's adsorptive nature may be concerned with ash content, because it exposes not only

Table 1 | Physicochemical properties of the BNH

	Weight % (on dry basis)	
Component	**BNH-AC**	**BNH**
Moisture content	7.81	9.90
Ash content	7.26	3.26
Volatile matter	40.76	60.16
Fixed carbon (yield)	44.17	26.68
Cellulose		46
Hemicellulose		19
Lignin		26
Extractives		9

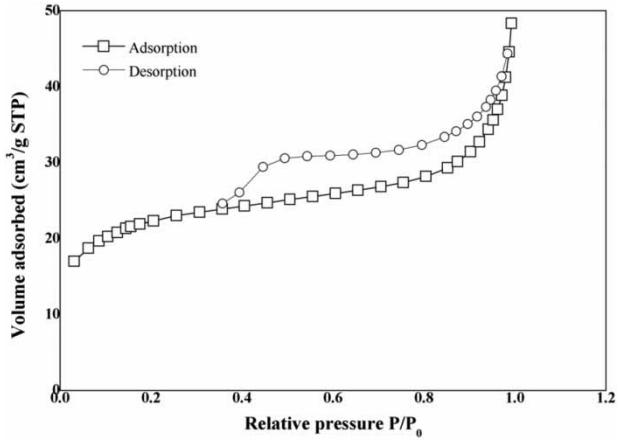

Figure 1 | N_2 adsorption-desorption isotherms of BNH-AC.

an inhibiting but also a stimulating characteristic in the case of adsorption of different organic chemicals (Wang *et al.* 2019). Moreover, it is directly related with AC pore structure (Anisuzzaman *et al.* 2014). In the current study, volatile matter of BNH-AC has a lower value compared to the raw BNH. Conversely, the ash content shows a higher ratio. Differently, the carbon content discloses the higher value in the case of BNH-AC (Table 1). Thus, this material is a good precursor.

Characterization of activated carbon

The textural properties of BNH-AC are determined by the BET surface area analysis. The surface area and total pore volume were found to be 81.73 m^2/g and 0.722 cm^3/g, respectively, and furthermore are larger than pyrolyzed areca husk (Subramani *et al.* 2019). The mean pore diameter was 3.533 nm. According to International Union of Pure and Applied Chemistry (IUPAC) classification, this pore diameter indicates the mesoporous properties (2.0 nm < d < 50 nm) (IUPAC 1972; Sing *et al.* 1985) and according to the new updated isotherm classification by IUPAC (Thommes *et al.* 2015), the isotherm is deemed to be a type IVa isotherm, one that indicates capillary condensation accompanied by hysteresis. Furthermore, type H_4 hysteresis loop was observed (Figure 1) which is very common in mesoporous carbon materials.

Figure 2 reveals the SEM micrographs of BNH, BNH-AC and the state of BNH-AC after adsorption at 3,000× magnification. Due to NaOH activator the pore areas are developed in Figure 2(b) in comparison with Figure 2(a) containing dense surface area. However, these large areas are refilled by cationic dye, i.e. MB. Therefore, Figure 2(c) shows a plane surface area. The activators' dehydration effect is responsible for the improved porosity. NaOH splits the C–O–C and C–O bonds of materials and is converted to Na (metallic), H_2 (gas) and sodium carbonate (Na_2CO_3). The equation is expressed as:

$$6NaOH + 2C \rightarrow 2Na + 3H_2 + 2Na_2CO_3 \quad (10)$$

Due to high temperature, in the existing N_2 gas, Na_2CO_3 is degraded into Na, CO and CO_2. Consequently, an ample number of voids has been constituted after trapping Na molecules in them (Hassan & Youssef 2014).

FTIR spectral analysis

FTIR spectra of raw BNH, BNH-AC and BNH-AC after adsorption are shown in Figure 3(a)–3(c), respectively. FTIR analysis determines the existing important functional groups like alkanes, esters, aromatics, ketones, alcohols and other oxygen-containing functional groups because of their concentrated lignocellulosic properties (Table 1). Adding or removing any functional groups reveals the changes occurring in the adsorption process after modifying the raw BNH to BNH-AC, which is visualized by band points in spectra. Two main peak regions are focused on the spectra of raw BNH: at low wavelength (600 – 1,800 cm^{-1}) and high wavelength (2,300 – 3,100 cm^{-1}). The peak points of 3,681.98 cm^{-1}, 3,750.11 cm^{-1} and 3,756.08 cm^{-1} in the spectra indicate the O – H stretching of alcohols and phenols, which are not clearly visualized in BNH-AC and after adsorption spectra. There are two main peaks observed on the surface of BNH and these present the alkanes (C–H stretching) and nitriles

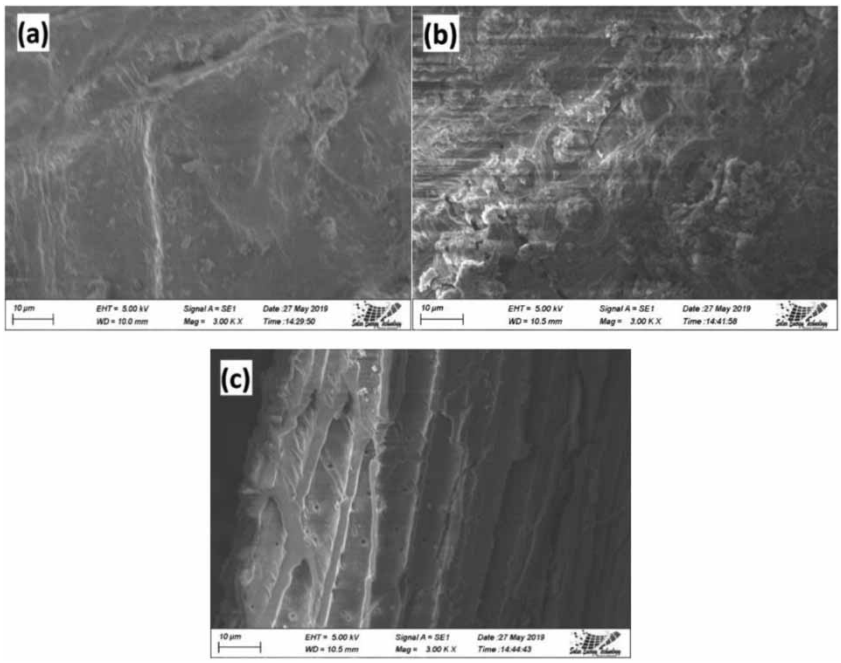

Figure 2 | SEM images of (a) BNH, (b) BNH-AC, (c) BNH-AC after adsorption.

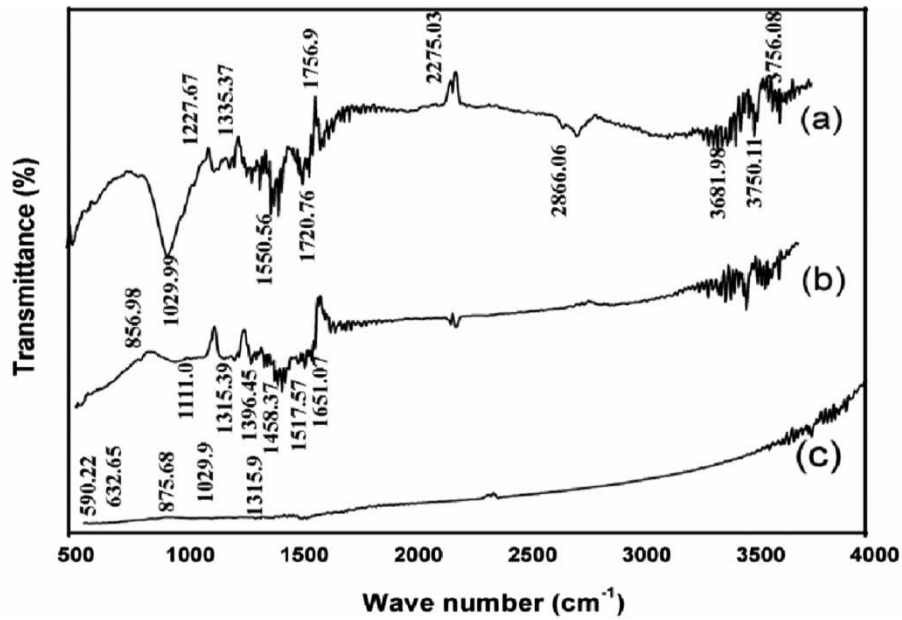

Figure 3 | FTIR spectra of (a) BNH, (b) BNH-AC, and (c) BNH-AC after adsorption.

(C≡N stretching) at 2,866.06 cm^{-1} and 2,275.03 cm^{-1}, respectively. After activation, these two peaks are shown to totally disappear from the spectrum after MB adsorption. However, a new peak (2,500 cm^{-1}) is observed in the BNH-AC after adsorption band corresponding to the O–H stretching of carboxylic acid (Islam *et al.* 2015).

A large number of peak points at 1,756.9 cm^{-1} and 1,720.76 cm^{-1}, 1,550.56 cm^{-1}, 1,335.37 cm^{-1}, 1,227.67 cm^{-1}, 1,029.99 cm^{-1} correspond to the C=O stretch (carboxylic acids, aldehydes), C–C stretch (aromatic), C–N stretch (aromatic amines), C–H (alkanes) and C–O stretch (alcohols, carboxylic acids, esters, ethers), respectively (Figure 3(a)).

Several functional groups remain constant after preparing AC, while 1,651.07 cm^{-1} and 856.98 cm^{-1} are noted as new peaks that indicate –C=C– stretch (alkanes) and =C–H bend (alkanes), respectively (Figure 3(b)). The dissipating of a large peak 1,029.99 cm^{-1} ascribed to the C–O stretch of alcohols, carboxylic acids, esters, ethers is noteworthy. In Figure 3(c), the immense band (600 – 1,800 cm^{-1}) mostly vanishes after MB adsorption except for some similar smaller peaks at 1,315.45 cm^{-1}, 1,029.99 cm^{-1} and 875.68 cm^{-1} that represent the C–N stretch (aromatic amines), C–O stretch (alcohols, carboxylic acids, esters, ethers) and =C–H bend (alkanes), respectively. The departure authenticates that the C=O and C–H are the active functional groups; perhaps these groups are engaged in the cationic MB dye and BNH-AC reaction. This type of phenomenon is confirmed by Islam *et al.* (2017b).

Adsorption studies

The MB dye's adsorption performance onto BNH-AC was conducted to determine the adsorption capacity at three different temperatures (30, 40 and 50 °C) and initial concentrations (25, 50, 100, 150, 200 and 250 mg/L). In Figure 4, adsorption capacity (q_t) of BNH-AC rises rapidly to 5 h in terms of higher concentrations occupying the void areas, whereas in low dye concentrations (25 and 50 mg/L), it rises slowly. The value of q_t increases when the dye concentration also increases. Overall, from all temperature graphs, we can conclude that the equilibrium capacity was obtained at 6 h, which supports other studies. According to Islam *et al.* (2017b), the MB adsorption capacity was attained at 8 h for rattan AC by NaOH activation. Available surface sites, is the main driving force for the dye removal, which remains in a large number at initial stage and is occupied with time. After arriving at equilibrium, this ratio declines, but due to the repulsion force between MB and the BNH-AC surface, some pore sites remain unfilled. Hence, the study lasted 24 h; it was valid and concurred with the findings of Ingole *et al.* (2017).

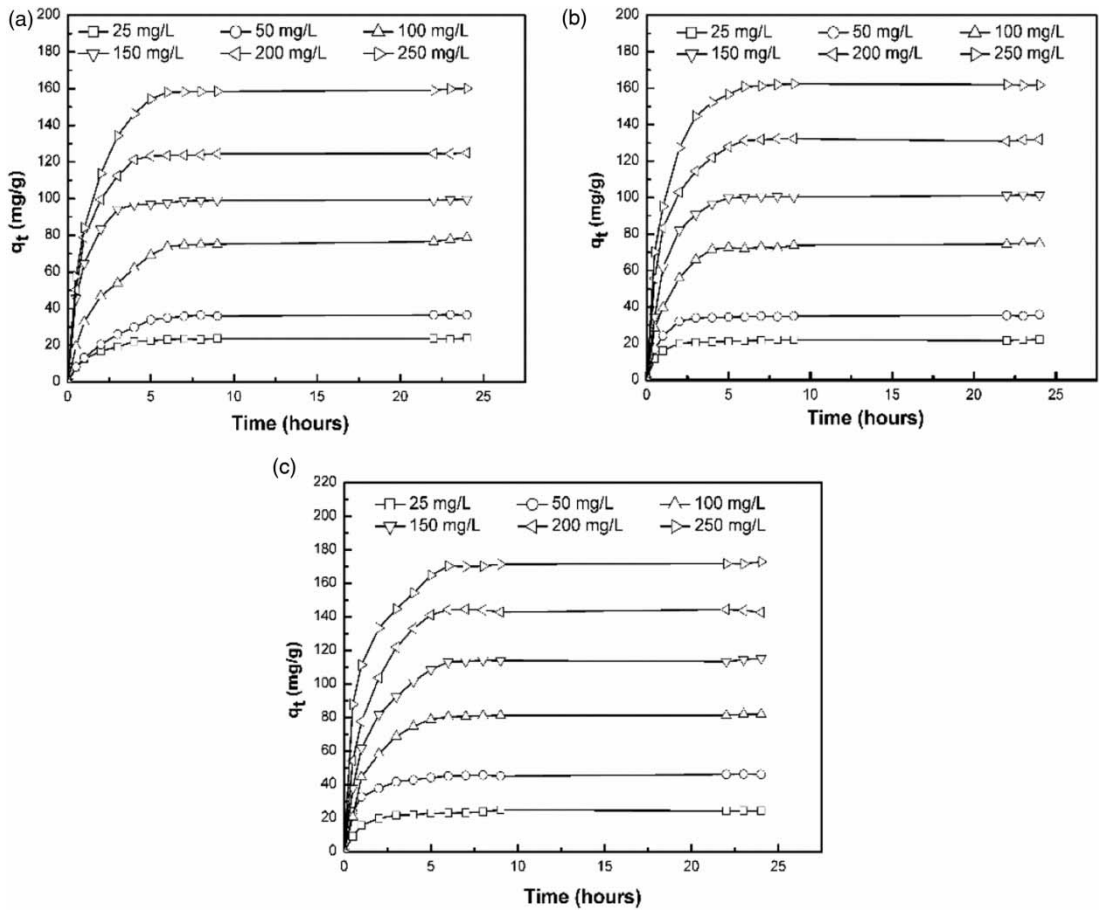

Figure 4 | Effect of contact time on adsorption capacity (q_t) of BNH-AC in different initial concentrations at (a) 30 °C, (b) 40 °C and (c) 50 °C (pH: 6.72, dose: 0.2 g).

Effect of pH

The pH_{pzc} exhibits a specific pH point where the net surface charge of adsorbent corresponds to zero, and it shows the possible mechanism for electrostatic interaction between adsorbent and adsorbate (Islam *et al.* 2015). The pH_{pzc} value of BNH-AC was obtained at 7.87 in this study (Figure 5(a)). This value indicates that the adsorbent surface area remains positively charged below this point, enhancing the conducive situation for anions. However, according to Islam *et al.* (2017b), the electrostatic interaction is likely to be escalated above this point.

The effect of pH on the adsorption process was observed at 40 °C. Basically, the main cause of this was due to the total adsorption process being in line with the Freundlich isotherm model, and the root mean square error (RMSE) at 40 °C was low compared to the other two temperatures, as shown in Table 2. Moreover, the treatments of industrial dye effluent are proceeded with at high temperature (Zou *et al.* 2018). The pH effect is illustrated by Figure 5(b), where pH ranged from 2 to 12 and the initial concentration of MB was 100 mg/L. From the figure, we can see that at low pH (pH = 2), the percentage removed remains low (77.59%) but increases simultaneously when the value of pH increases. The main logic behind this is the oxygen-containing functional groups (–COOH, –OH) of BNH-AC. In acidic pH, the oxygen-containing functional groups are protonated to the cationic form, like $–COOH_2^+$, $–OH_2^+$, which releases the number of negative charges. Thus, the surface sites do not favor binding the cationic dye and resulted in an electrostatic repulsion causing poor removal (%). Conversely, such functional groups are deprotonated to anionic form ($–COO^-$, $–O^-$) with increasing the basic condition. Thus, it creates electrostatic force with the cationic dye and makes the surface more favorable to adsorption (Konicki *et al.* 2017).

Table 2 | Langmuir and Freundlich isotherm parameters (non-linear) for adsorption of MB onto BNH-AC at different temperatures

		Temperature (°C)		
Model	**Parameter**	**30**	**40**	**50**
Langmuir	q_m (mg/g)	381.6	339.8	235.2
	K_a (L/mg)	0.007	0.009	0.028
	R^2	0.9741	0.9841	0.9999
	RMSE	4.664	3.837	0.265
Freundlich	K_F (mg/g (L/mg)$^{1/n}$)	16.03	7.95	6.19
	1/n	0.669	0.660	0.535
	R^2	0.9946	0.9992	0.9985
	RMSE	2.129	0.842	1.216

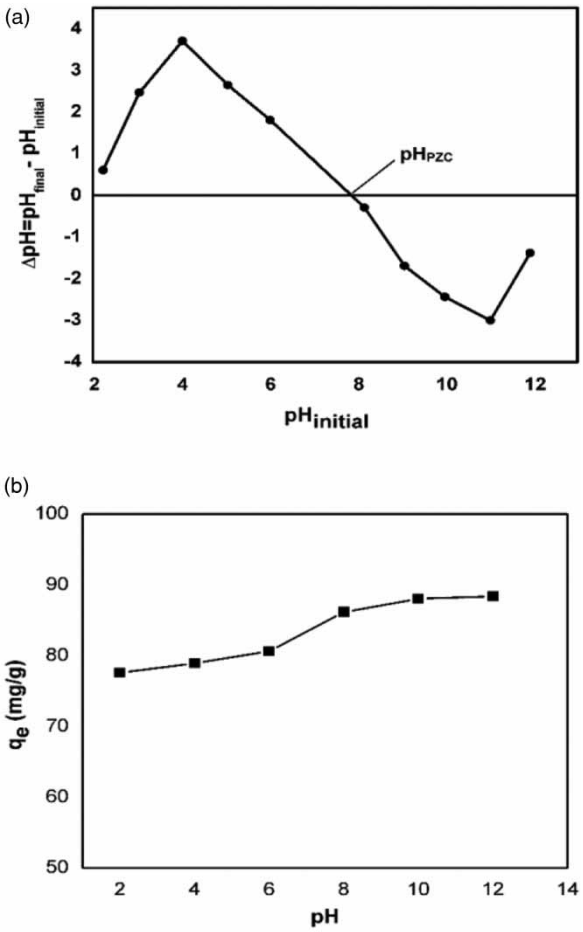

Figure 5 | (a) pH_{pzc} of BNH-AC, (b) effect of pH on MB removal by BNH-AC at 40 °C.

Adsorption isotherms

The interaction of adsorbate with adsorbents and the equilibrium distributions of adsorbate molecules between the solid and liquid phases are known as adsorption isotherms (Islam *et al.* 2017a). To determine the further adsorption equilibrium, two famous isotherm equations, Langmuir (Langmuir 1918) and Freundlich (Freundlich 1906), were applied to fit the experimental equilibrium isotherm data of MB adsorption on BNH-AC. The single layer adsorption process on consistent adsorption sites is narrated by the Langmuir isotherm model, while the multilayer adsorption process on different adsorption sites is described by the Freundlich isotherm model.

These two models are mathematically expressed as:

$$\text{Langmuir isotherm: } q_e = \frac{q_m K_a C_e}{1 + K_a C_e} \quad (11)$$

$$\text{Linear form: } \frac{C_e}{q_e} = \frac{C_e}{q_m} + \frac{1}{K_L q_m} \quad (12)$$

where, q_e (mg/g) represents the adsorption capacity at equilibrium, C_e (mg/L) is the equilibrium dye concentration, and q_m is the maximum adsorption capacity. K_a(1/mg) and K_L (L/mg) stand for the Langmuir constant and the constant of free energy of adsorption process, respectively:

$$\text{Freundlich isotherm: } q_e = K_F C_e^{1/n} \quad (13)$$

$$\text{Linear form: } \ln q_e = \ln K_F + \frac{1}{n} \ln C_e \quad (14)$$

where, K_F (mg/g (L/mg)$^{1/n}$) and n are Freundlich constants representing the adsorption capacity and the intensity of adsorption, respectively.

By plotting q_e and C_e, the adsorption isotherm was attained and is shown in Figure 6(a). Furthermore, out of these two models, the best suited isotherm model was

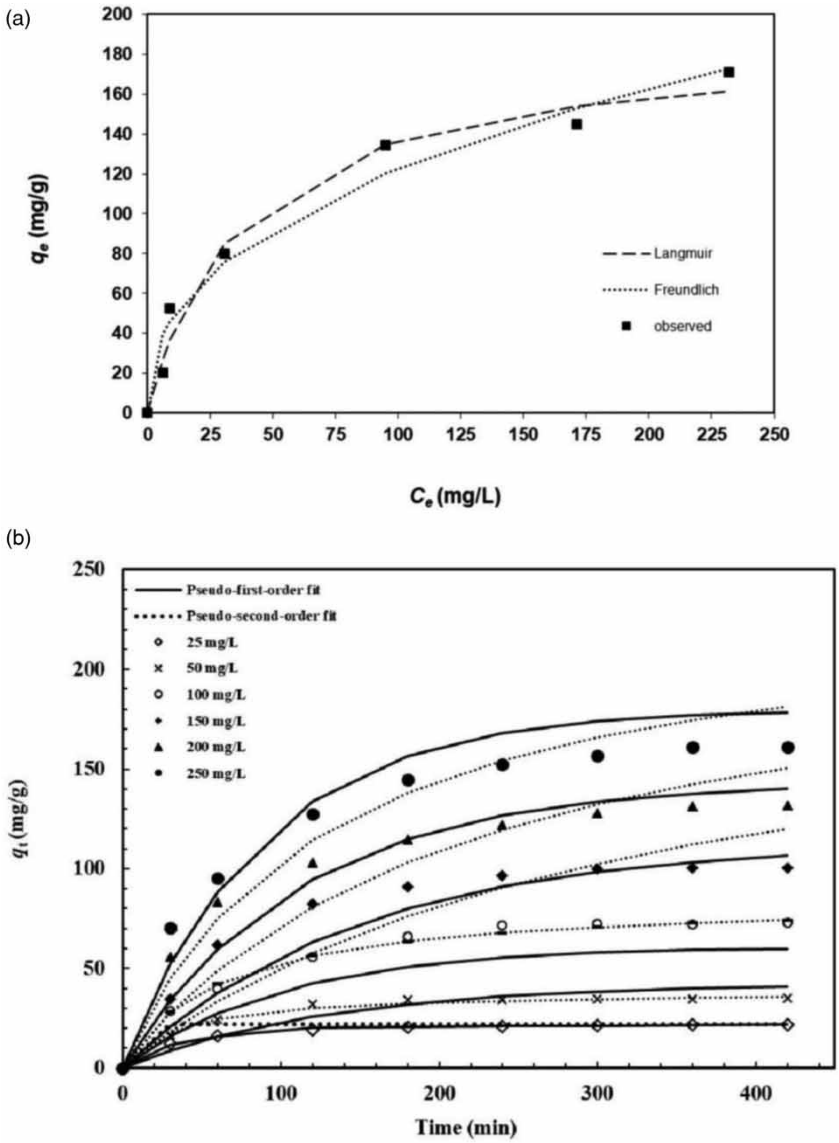

Figure 6 | (a) Adsorption isotherm curve of the Langmuir and Freundlich models, (b) non-linear plots of the pseudo-first- and pseudo-second-order kinetic models for MB adsorption on BNH-AC at 40 °C.

recognized by the R^2 value and also authenticated by the RMSE value. Both of these are numerically expressed as:

$$R^2 = 1 - \frac{\sum_{n-1}^{n} (q_{e.meas} - q_{e.cal)}^2}{\sum_{n-1}^{n} (q_{e.meas} - \overline{q_{e.cal}})^2} \quad (15)$$

$$RMSE = \sqrt{\frac{1}{n-1} \sum_{n-1}^{n} (q_{e.meas} - q_{e.cal})^2} \quad (16)$$

Here, $q_{e.meas}$ (mg/g) and $q_{e.cal}$ (mg/g) are the experimental and predicted value of adsorption capacity at equilibrium. The number of observations is presented by 'n'.

Table 2 exhibits the non-linear calculated value of two isotherm models. The Freundlich isotherm model shows the highest R^2 value and lower RMSE compared to the Langmuir model. That means the adsorption process can be better described by the Freundlich model where adsorption appeared on heterogeneous sites and revealed high adsorption capacities. Moreover, the non-linear calculated q_m was found to be 381.6, 339.8 and 235.2 mg/g at 30, 40 and 50 °C, respectively, which is higher than any other materials, like cotton stalk activated by KOH and K_2CO_3 ($q_m = 294.12$ and 285.71 mg/g, respectively) (Deng *et al.* 2010), karanj fruit hull activated by KOH ($q_m = 239.40$ mg/g) (Islam *et al.* 2017a), rattan palm tree activated by NaOH (359 mg/g) (Islam *et al.* 2017b) and so on. We can deduce that BNH as a precursor can be feasibly employed for manufacturing an efficacious and productive AC.

The values of the Freundlich constant 1/n were less than 1, and this indicates a supportive adsorption process. If these values are near zero, the adsorption heterogenicity will be higher. This finding coincides with various studies where the Freundlich model fitted better than the Langmuir model. Examples are NaOH-activated palm date seed (Islam *et al.* 2015), ion beam-modified palygorskite (Zhang *et al.* 2013), amino-modified mesostructured silica nanoparticles (Karim *et al.* 2012) and many more. Therefore, some heterogenicity is placed on the surface sites of BNH-AC, which is responsible for MB adsorption.

Adsorption kinetics

Kinetic studies are required to understand the adsorption mechanism as well as the rate of adsorption. Pseudo-first-order and pseudo-second order kinetic models have been devised to describe the potential adsorption dynamics. Pseudo-first order kinetic model was suggested by Lagergren and Svenska (Lagergren 1898), who mathematically expressed the non-linear form as:

$$q_t = q_e(1 - exp^{-k_1 t}) \quad (17)$$

q_t and q_e of this equation are adsorption capacity of BNH-AC at time, t (min) and at equilibrium, respectively, k_1 is rate constant of the adsorption (1/min) of the pseudo-first-order kinetic model. The non-linear pseudo-second-order equation (Ho & McKay 1998) is:

$$q_t = \frac{q_e^2 k_{2t}}{1 + q_e k_{2t}} \quad (18)$$

where, k_2 (g/mg·min) is the rate constant of pseudo-second-order adsorption. The best-fitted model between these two was obtained by calculating the coefficient of determination (R^2) and two non-linear error functions: normalized standard deviation (NSD) and average relative error (ARE). These are articulated as follows:

$$R^2 = 1 - \frac{\sum_{n=1}^{n} (q_{e.exp} - q_{e.mod})^2}{\sum_{n=1}^{n} (q_{e.exp} - \overline{q_{e.mod}})^2} \quad (19)$$

$$NSD = 100 \times \sqrt{\frac{1}{n-1} \sum_{i=1}^{n} \left[\frac{q_{t.exp} - q_{t.mod}}{q_{t.exp}}\right]^2} \quad (20)$$

$$ARE = \frac{100}{n} \sum_{i=1}^{n} \left[\frac{q_{t.exp} - q_{t.mod}}{q_{t.exp}}\right] \quad (21)$$

where, $q_{t.exp}$ (mg/g) is the experimental adsorption capacity value at time t and $q_{t.mod}$ (mg/g) represents the model-anticipated value of adsorbed amount MB dye at time t. The higher value of R^2 and lower value of NSD and ARE demonstrate the best-suited model.

The non-linear plot of the pseudo-first- and second-order fitting and experimental kinetic values is presented in Figure 6(b). This figure displays the obtained equilibrium at 6 h, which means the dye adsorbing rate was equal to the dye desorbing rate after achieving its saturation level. The analyzed kinetic parameters using the non-linear method are summarized in Table 3. Referring to the different dye concentrations, the pseudo-second-order model shows high R^2 values with low NSD and ARE values compared to pseudo-first-order kinetics. Even the modeled value of q_e (mg/g) is best fitted with experimental q_e (mg/g) value in pseudo-second-order kinetics. All the outcomes cited above prove that the adsorption of MB dye on to BNH-AC follows the pseudo-second-order model, so

Table 3 | Kinetic parameters for adsorption of MB onto BNH-AC at different initial concentrations

	C_0 (mg/L)					
Parameters	**25**	**50**	**100**	**150**	**200**	**250**
q_{eexp} (mg/g)	21.5	34.592	71.993	100.226	131.272	160.833
Pseudo-first-order						
q_e (mg/g)	21.874	42.656	60.909	113.199	143.261	179.970
k_1 (1/min)	0.410	0.008	0.009	0.007	0.009	0.011
R^2	0.512	0.036	0.239	0.669	0.761	0.776
NSD	5.35	49.382	59.542	40.922	27.098	3.128
ARE	22.051	0.486	53.613	20.709	4.365	13.783
Pseudo-second-order						
q_e (mg/g)	23.411	38.482	84.968	211.919	230.012	236.967
k_2 (g/mg min)	0.002	0.001	0.0002	0.00001	0.00002	0.00003
R^2	0.985	0.965	0.980	0.852	0.757	0.7088
NSD	4.673	1.128	2.498	33.258	24.213	18.524
ARE	0.083	0.232	0.003	10.681	8.881	0.799

chemisorption is supported and not physisorption. This study agrees with the findings of other analyses, such as adsorption on cabbage waste powder (Wekoye *et al.* 2020) and white sugar AC (Xiao *et al.* 2020). Table 4 represents a comparative study of several previous precursors with the present study in terms of MB adsorption. Table 4 disclosed that the q_m of the Mangoosteen peel is 1,193 mg/g, which represents a higher value due to large surface area (1,622 m^2/g) and mesoporous characteristics (Nasrullah *et al.* 2019). However, the q_m of BNH-AC reveals higher value compared with other precursors (Table 4).

Adsorption mechanism

Kinetic studies cannot describe the mechanism of the adsorption process; they can merely interpret the solute–

Table 4 | Comparison of BNH-AC with previous adsorption studies with respect to methylene blue removal

							Fitted model		
Sorbent	**Activating agent**	**T (°C)**	**pH**	**Time (h)**	**Dose (gm/L)**	**q_m (mg/g)**	**Isotherm**	**Kinetic**	**References**
Mangoosteen peel	$ZnCl_2$	25	9	10	0.33	1,193	Langmuir	Pseudo-second-order	Nasrullah *et al.* (2019)
Sargassum hemiphyllum		30	5	2	0.5	729.93	Langmuir	Pseudo-second-order	Liang *et al.* (2017)
Coffee husk	KOH	30	7	12	1	416.68	Langmuir	Pseudo-second-order	Tran *et al.* (2020)
Dipterocarpus alatus fruit	$ZnCl_2$		6.5	3	0.2	269.30	Langmuir	Pseudo-second-order	Patawat *et al.* (2020)
Eucalyptus sheathiana bark		30		2.33		204.08	Langmuir	Pseudo-second-order	Afroze *et al.* (2016)
Pumpkin peel	NaOH	30	11	3	0.5	169	Langmuir	Pseudo-second-order	Rashid *et al.* (2019)
Fallen coconut leaves	KOH	30	6		1	147.10	Langmuir	Pseudo-second-order	Rashid *et al.* (2016)
Kendu fruit peel	$(NH_4)_2CO_3$		≥ 6	1.67	0.1	144.90	Langmuir	Pseudo-second-order	Sahu *et al.* (2020)
Apricot stone	H_3PO_4	25	10	0.67	1	46.30	Langmuir	Pseudo-second-order	Abbas & Trari (2020)
Grape stalks powder			12.97	4.33	9.98	7.81	Langmuir	Pseudo-second-order	Davarnejad *et al.* (2020)
Rubber seed shell	KOH		6	1	50			Pseudo-second-order	Azani *et al.* (2019)
BNH-AC	NaOH	30	10	6	1	381.60	Freundlich	Pseudo-second-order	Present study

surface interactions during adsorption. There are some important steps for MB adsorption on BNH-AC and they are (a) film diffusion, (b) pore diffusion, (c) surface diffusion, and (d) adsorption on the pore surface. Therefore, the Weber–Morris intraparticle diffusion and Boyd models were used to analyze such kinds of adsorption mechanisms.

The Weber–Morris intraparticle diffusion (Weber & Morris 1963), which is attained from Fick's second law of diffusion, can be written as:

$$q_t = k_{id} t^{\frac{1}{2}} + C \tag{22}$$

where, k_{id} and C are the intraparticle diffusion rate constant (mg/g. $min^{1/2}$) and intercept related to the boundary layer effect (mg/g), respectively. In Figure 7(a), linear plots of q_t

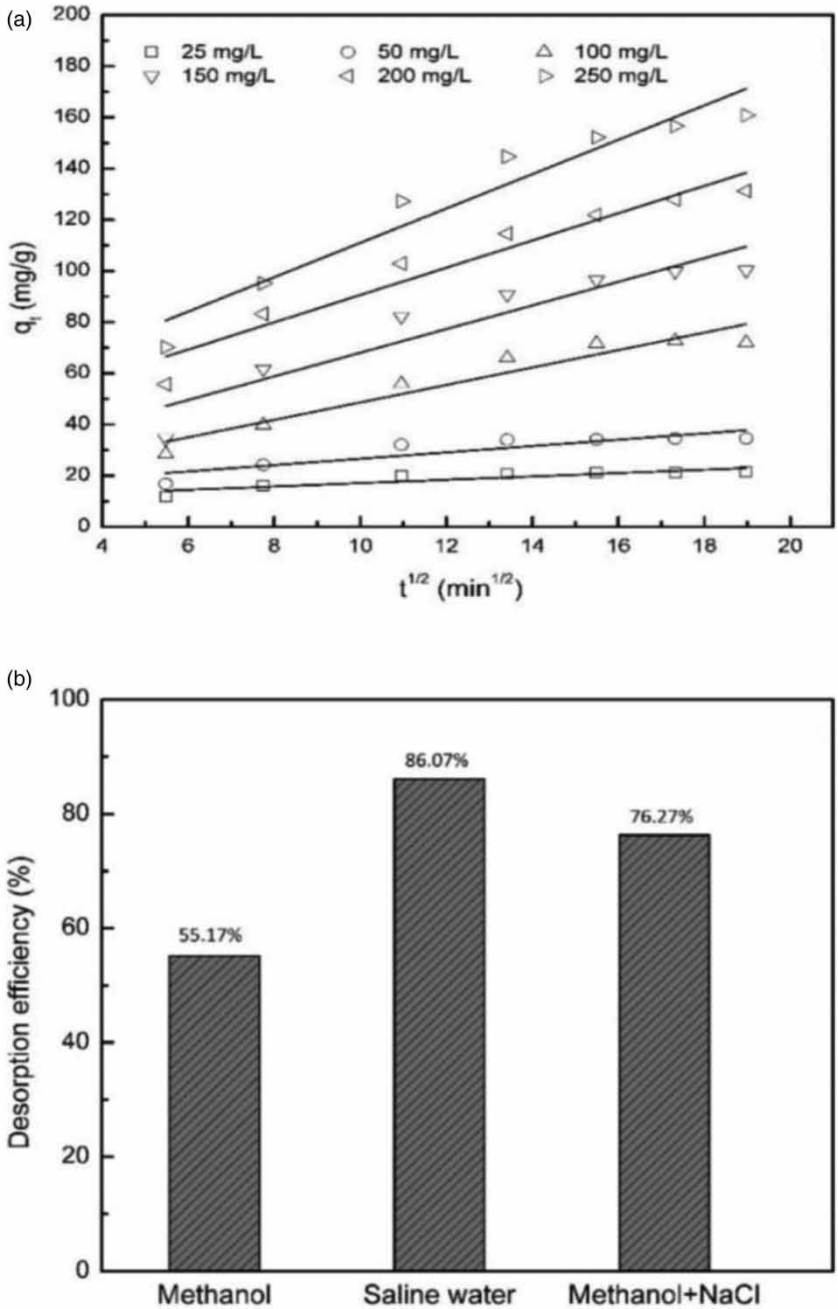

Figure 7 | (a) Intraparticle diffusion model for MB adsorption on BNH-AC, (b) comparison of desorption efficiency (%) in different media.

versus $t^{1/2}$, the gradient and intercept values are the expression of k_{id} and C. From the graphical representation, we can observe that the pore and intraparticle diffusion increased with an increase in the initial MB concentrations (25 mg/L–250 mg/L). The Boyd model (Boyd *et al.* 1947) could differentiate intraparticle and film diffusion and is linearly expressed as:

$$\ln\left(1 - \frac{q_t}{q_e}\right) = -k_{fd}t \tag{23}$$

where, k_{fd} is the liquid film diffusion constant obtained from the linear plotting of ln $(1 - q_t/q_e)$ vs. t.

Table 5 illustrates the value of intraparticle as well as film diffusion for adsorption of MB dye on to BNH-AC for different initial concentrations. As the value of C defines the boundary layer effect, the higher values confirm the higher effect. If the plotted lines pass through the origin, then it can be said that intraparticle diffusion controls the adsorption process. Nevertheless, in most cases the plotting lines do not pass through the origin, which corresponds to different mechanisms rather than intraparticle diffusion controlling the adsorption process (Figure 7(a)). Hence, film diffusion, the slow movement of solutes from the boundary layer to the adsorbent's surface, might be responsible for controlling MB adsorption. Even the R^2 values of the intraparticle diffusion model are lower than the Boyd model (Table 5) and this coincides with the findings. Similar studies were done by Njoku *et al.* (2014) for carbofuran insecticide by coconut frond AC.

Adsorption thermodynamics

The thermodynamic parameters for adsorption consist of Gibbs free energy change (G°), enthalpy change (H°), and entropy change (S°), which can be calculated by:

$$\ln k_d = \frac{\Delta S^\circ}{R} - \frac{\Delta H^\circ}{RT} \tag{24}$$

$$\Delta G^\circ = -RT \ln K_d \tag{25}$$

where, R is the universal gas constant (8.314 J/mol K) and T is the absolute temperature (K), respectively. K_d demonstrates the adsorption distribution constant (1/mg), which can be expressed as:

$$K_d = \frac{C_{Ae}}{C_e} \tag{26}$$

where, C_{Ae} denotes the amount of MB dye adsorbed at equilibrium and C_e is the equilibrium concentrations of the MB dye (mg/L).

Table 6 computes the thermodynamic parameters, where ΔG° implies negative values. It supports the remarkable spontaneity of the adsorption process and significant amount of energy being generated (Njoku *et al.* 2014). As well, these values decrease when the temperature rises, demonstrating that the adsorption of MB on to BNH-AC is thermodynamically conducive at high temperature. The ΔH° value also provides the negative sign indicating the exothermic nature of the adsorption process. The decreased attraction between MB molecules and the active surface sites on the BNH-AC with rising temperature could also explain the findings, which eventually decreased the adsorption capacity. The positive sign of ΔS° indicates the randomness of the adsorption system, which provides superior attraction between adsorbate molecules and adsorbent surface sites. Islam *et al.* (2015) reported an analogous study for palm date seed AC for ΔG°, ΔH° and ΔS°. Basically, such kinds of results are a common outcome of physical

Table 5 | Intraparticle diffusion and film diffusion parameters for adsorption of MB onto BNH-AC at different initial concentrations

	C_o (mg/L)					
Parameters	**25**	**50**	**100**	**150**	**200**	**250**
Intraparticle diffusion model						
K_{id}	0.654	1.238	3.406	4.62	5.327	6.712
C	10.538	14.236	14.574	21.857	37.342	43.875
R^2	0.804	0.796	0.923	0.884	0.937	0.936
Film diffusion model						
K_{fd}	0.013	0.019	0.021	0.017	0.011	0.011
R^2	0.956	0.97	0.892	0.94	0.984	0.999

Table 6 | Thermodynamic parameters for adsorption of MB onto BNH-AC

ΔG° (kJ/mol)		ΔH° (kJ/mol)	ΔS° (kJ/mol.K)
303.13	−12.7165		
313.15	−13.0281	−2.4274	0.0338
323.15	−13.349		

adsorption, something that can take place through electrostatic interactions.

Desorption study

Desorption performance refers to clarifying not only the overall sorption mechanism but also recovery of the used adsorbent material (Yu *et al.* 2011). It is essential to know the desorption efficiency of separate media, as this can suggest the suitable eluent for regeneration studies. In the present work, three media were used for the MB desorption study: methanol (CH_3OH), sodium chloride (0.1 mol/dm^3) in methanol, and sodium chloride (0.1 mol/dm^3) in water, as recommended by Moreira *et al.* (2017). The desorption study was carried out in a batch experiment mode at adsorption equilibrium state (initial concentration = 100 mg/L; temperature = 30 °C; time = 6 h). According to Figure 7(b), saline water (NaCl + H_2O) is the most efficient eluent of the three solutions, showing 86.07% desorption efficiency. On the other hand, a combination of NaCl and methanol shows a noticeable desorption potential (76.27%) compared to only methanol. Previously, NaCl solution has proven to be suitable media for desorption of cationic dye (malachite green) where a high concentration of NaCl solution enhanced dye desorption due to its ionic strength (Jiang *et al.* 2017). This high ionic strength splits the electrostatic bindings between positive MB dye and adsorbent, which stimulates the MB dye removal. This finding is due to using saline water, and BNH-AC can be handily regenerated for further dye removal application.

CONCLUSION

The potential of BNH as a new and economically efficient raw material for AC was explored in the present study. Various authenticated and well-known numerical models and settings were adopted to compare the experimental findings. The significant adsorption capacity (q_m) of BNH-AC was found as 381.6, 339.8 and 235.2 mg/g at 30, 40 and 50 °C, respectively, by using the non-linear calculation of the conventional isotherm model. Also the Freundlich isotherm model proved to be the best-suited model for the isotherm study due to its high R^2 value. Meanwhile, pseudo-second-order kinetics explained the adsorption kinetic model as revealed in this study. Due to the electrostatic force increasing with a basic pH level, the removal of MB was higher at a pH value of 10 and this remained constant from pH 10 to 12. In accordance with the fitting on the Weber–Morris intraparticle diffusion and Boyd models, solutes' low motion from the boundary layer to the BNH-AC surface was proved, followed by film diffusion rather than intraparticle diffusion. Moreover, the thermodynamic studies indicated that the adsorption process was spontaneous and exothermic. C=O and C–H were the active functional groups, engaged in the reaction of cationic MB dye and BNH-AC. This was authenticated by FTIR spectral analysis. Finally, the above mentioned findings confirmed that BNH-AC, using NaOH activation, can be an efficiently advanced adsorbent for removing environmental pollutants.

ACKNOWLEDGEMENTS

This study was supported by the University Grant Commission, Bangladesh.

DATA AVAILABILITY STATEMENT

All relevant data are included in the paper or its Supplementary Information.

REFERENCES

Abbas, M. & Trari, M. 2020 Removal of methylene blue in aqueous solution by economic adsorbent derived from apricot stone activated carbon. *Fibers and Polymers* **21**, 810–820.

Afroze, S., Sen, T. K., Ang, M. & Nishioka, H. 2016 Adsorption of methylene blue dye from aqueous solution by novel biomass *Eucalyptus sheathiana* bark: equilibrium, kinetics, thermodynamics and mechanism. *Desalination and Water Treatment* **57** (13), 5858–5878.

Ahmad, T., Danish, M., Rafatullah, M., Ghazali, A., Sulaiman, O., Hashim, R., Nasir, M. & Ibrahim, M. 2012 The use of date palm as a potential adsorbent for wastewater treatment: a review. *Environmental Science and Pollution Research* **19**, 1464–1484.

Anisuzzaman, S. M., Krishnaiah, D., Abang, S. & Labadin, G. M. 2014 Adsorptive denitrogenation of fuel by oil palm shells as low cost adsorbents. *Journal of Applied Science* **14** (23), 3156–3161.

Azani, M., Silmi, N. F., Chuin, C. T. H., Abdullah, N. S., Sharifuddin, S. S. & Hussin, M. H. 2019 Characterisation and kinetic studies on activated carbon derived from rubber seed shell for the removal of methylene blue in aqueous solutions. *Journal of Physical Science* **30** (2), 1–20.

Baumer, J. D., Valério, A., de Souza, S. M. A. G. U., Erzinger, G. S., Furigo, A. & de Souza, A. A. U. 2018 Toxicity of enzymatically decolored textile dyes solution by horseradish peroxidase. *Journal of Hazardous Materials* **360**, 82–88.

Borah, J. & Dutta, N. 2018 Development and properties evaluation of betel nut fibres composite material. *Materialstoday: Proceedings* **5** (1), 2229–2233.

Boyd, G. E., Adamson, A. W. & Myers, L. S. 1947 The exchange adsorption of ions from aqueous solutions by organic zeolites. II. Kinetics. *Journal of American Chemical Society* **69** (11), 2836–2848.

Cao, C., Xiao, L., Chen, C., Shi, X., Cao, Q. & Gao, L. 2014 In situ preparation of magnetic Fe_3O_4/chitosan nanoparticles via a novel reduction–precipitation method and their application in adsorption of reactive azo dye. *Powder Technology* **260**, 90–97.

Cazetta, A. L., Vargas, A. M. M., Nogami, E. M., Kunita, M. H., Guilherme, M. R., Martins, A. C., Silva, T. L., Moraes, J. C. G. & Almeida, V. C. 2011 NaOH-activated carbon of high surface area produced from coconut shell: kinetics and equilibrium studies from the methylene blue adsorption. *Chemical Engineering Journal* **174** (1), 117–125.

Chandra, C. S. J., George, N. & Narayanankutty, S. K. 2016 Isolation and characterization of cellulose nanofibrils from arecanut huskfibre. *Carbohydrate Polymers* **142**, 158–166.

Chen, L., Li, D., Huang, Y., Zhu, W., Ding, Y. & Guo, C. 2020 Preparation of sludge-based-hydrochar at different temperatures and adsorption of BPA. *Water Science and Technology* **82** (2), 255–265.

Das, M., Samal, A. K. & Mehar, N. 2020 *Butea monosperma* leaf as an adsorbent of methylene blue: recovery of the dye and reuse of the adsorbent. *International Journal of Environmental Science and Technology* **17**, 2105–2112.

Davarnejad, R., Afshar, S. & Etehadfar, P. 2020 Activated carbon blended with grape stalks powder: properties modification and its application in a dye adsorption. *Arabian Journal of Chemistry* **13** (5), 5463–5473.

Deng, H., Li, G., Yang, H., Tang, J. & Tang, J. 2010 Preparation of activated carbons from cotton stalk by microwave assisted KOH and K_2CO_3 activation. *Chemical Engineering Journal* **163** (3), 373–381.

Dey, M. D., Ahmed, M., Singh, R., Boruah, R. & Mukhopadhyay, R. 2017 Utilization of two agrowastes for adsorption and removal of methylene blue: kinetics and isotherm studies. *Water Science and Technology* **75** (5), 1138–1147.

Freundlich, H. 1906 Über die adsorption in lösungen (adsorption in solution). *PhysikalischeChemie* **57**, 384–470.

Hassan, A. F. & Youssef, A. M. 2014 Preparation and characterization of microporous NaOH-activated carbons from hydrofluoric acid leached rice husk and its application for lead (II) adsorption. *Carbon Letters* **15** (1), 57–66.

Hassan, M. M., Wagner, M. H., Zaman, H. U. & Khan, M. A. 2010 Physico-Mechanical performance of hybrid betel Nut (*Areca catechu*) short fiber/Seaweed polypropylene composite. *Journal of Natural Fibers* **7** (3), 165–177.

Heidarinejad, Z., Dehghani, M. H., Heidari, M., Javedan, G., Ali, I. & Sillanpää, M. 2020 Methods for preparation and activation of activated carbon: a review. *Environmental Chemistry Letters* **18**, 393–415.

Ho, Y. S. & McKay, G. 1998 Sorption of dye from aqueous solution by peat. *Chemical Engineering Journal* **70** (2), 115–124.

Hoque, A. & Clarke, A. 2013 Greening of industries in Bangladesh: pollution prevention practices. *Journal of Cleaner Production* **51**, 47–56.

Illingworth, J. M., Rand, B. & Williams, P. T. 2019 Non-woven fabric activated carbon produced from fibrous waste biomass for sulphur dioxide control. *Process Safety and Environmental Protection* **122**, 209–220.

Ingole, R. S., Lataye, D. H. & Dhorabe, P. T. 2017 Adsorption of phenol onto banana peels activated carbon. *KSCE Journal of Civil Engineering* **21** (1), 100–110.

Islam, M. M., Mahmud, K., Faruk, O. & Billah, M. S. 2011 Textile dyeing industries in Bangladesh for sustainable development. *International Journal of Environmental Science and Development* **2** (6), 428.

Islam, M. A., Tan, I. A. W., Benhouria, A., Asif, M. & Hameed, B. H. 2015 Mesoporous and adsorptive properties of palm date seed activated carbon prepared via sequential hydrothermal carbonization and sodium hydroxide activation. *Chemical Engineering Journal* **270**, 187–195.

Islam, M. A., Sabar, S., Benhouria, A., Khanday, W. A., Asif, M. & Hameed, B. H. 2017a Nanoporous activated carbon prepared from karanj (*Pongamia pinnata*) fruit hulls for methylene blue adsorption. *Journal of the Taiwan Institute of Chemical Engineers* **74**, 96–104.

Islam, M. A., Ahmed, M. J., Khanday, W. A., Asif, M. & Hameed, B. H. 2017b Mesoporous activated carbon prepared from NaOH activation of rattan (*Lacosperma secundiflorum*) hydrochar for methylene blue removal. *Ecotoxicology and Environmental Safety* **138**, 279–285.

IUPAC 1972 Manual of symbols and terminology. *Pure and Applied Chemistry* **31**, 587.

Jamee, R. & Siddique, R. 2019 Biodegradation of synthetic dyes of textile effluent by microorganisms: an environmentally and economically sustainable approach. *European Journal of Microbiology and Immunology* **9** (4), 114–118.

Jawad, A. H., Sabar, S., Ishak, M. A. M., Wilson, L. D., Norrahma, S. S. A., Talaria, M. K. & Farhan, A. M. 2017 Microwave-assisted preparation of mesoporous-activated carbon from coconut (*Cocos nucifera*) leaf by H_3PO_4 activation for methylene blue adsorption. *Chemical Engineering Communications* **204** (10), 1143–1156.

Jawad, A. H., Ismail, K., Ishak, M. A. M. & Wilson, L. D. 2018 Conversion of Malaysian low-rank coal to mesoporous activated carbon: structure characterization and adsorption properties. *Chinese Journal of Chemical Engineering* **27** (7), 1716–1727.

Jiang, F., Dinh, D. M. & Hsieh, Y.-L. 2017 Adsorption and desorption of cationic malachite green dye on cellulose nanofibril aerogels. *Carbohydrate Polymers* **173**, 286–294.

Kafshgari, L. A., Ghorbani, M., Azizi, A., Agarwal, S. & Gupta, V. K. 2017 Modeling and optimization of direct red 16 adsorption from aqueous solutions using nanocomposite of $MnFe_2O_4$/MWCNTs: RSM-CCRD model. *Journal of Molecular Liquids* **233**, 370–377.

Karim, A. H., Jalil, A. A., Triwahyono, S., Sidik, S. M., Kamarudin, N. H. N., Jusoh, R., Jusoh, N. W. C. & Hameed, B. H. 2012 Amino modified mesostructured silica nanoparticles for efficient adsorption of methylene blue. *Journal of Colloid and Interface Science* **386** (1), 307–314.

Kaya, N. & Uzun, Y. Z. 2020 Investigation of effectiveness of pyrolysis products on removal of alizarin yellow GG from aqueous solution: a comparative study with commercial activated carbon. *Water Science and Technology* **81** (6), 1191–1208.

Kaykhaii, M., Sasani, M. & Marghzari, S. 2018 Removal of dyes from the environment by adsorption process. *Chemical and Materials Engineering* **6** (2), 31–35.

Khan, S. & Malik, A. 2014 Environmental and Health Effects of Textile Industry Wastewater. In: *Environmental Deterioration and Human Health* (A. Malik, E. Grohmann & R. Akhtar eds). Springer, Dordrecht.

Konicki, W., Aleksandrzak, M. & Mijowska, E. 2017 Equilibrium, kinetic and thermodynamic studies on adsorption of cationic dyes from aqueous solutions using graphene oxide. *Chemical Engineering Research and Design* **123**, 35–49.

Kuppusamy, S., Venkateswarlu, K., Thavamani, P., Lee, Y. B., Naidu, R. & Megharaj, M. 2017 *Quercus robur* acorn peel as a novel coagulating adsorbent for cationic dye removal from aquatic ecosystems. *Ecological Engineering* **101**, 3–8.

Lagergren, S. 1898 Zurtheorie der sogenannten adsorption gelösterstoffe. *KungligaSvenskaVetenskapsakademiens. Handlingar* **24**, 1–39.

Langmuir, I. 1918 The adsorption of gases on plane surfaces of glass, mica and platinum. *Journal of American Chemical Society* **40** (9), 1361–1403.

Liang, J., Xia, J. & Long, J. 2017 Biosorption of methylene blue by nonliving biomass of the brown macroalga *Sargassum hemiphyllum*. *Water Science and Technology* **76** (6), 1574–1583.

Liew, R. K., Chong, M. Y., Osazuwa, O. U., Nam, W. L., Phang, X. Y., Su, M. H., Cheng, C. K., Chong, C. T. & Lam, S. S. 2018 Production of activated carbon as catalyst support by microwave pyrolysis of palm kernel shell: a comparative study of chemical versus physical activation. *Research on Chemical Intermediates* **44**, 3849–3865.

Melliti, A., Kheriji, J., Bessaies, H. & Hamrouni, B. 2020 Boron removal from water by adsorption onto activated carbon prepared from palm bark: kinetic, isotherms, optimisation and breakthrough curves modeling. *Water Science and Technology* **81** (2), 321–332.

Moreira, M. A., Ciuffi, K. J., Rives, V., Vicente, M. A., Trujillano, R., Gil, A., Korili, S. A. & de Faria, E. H. 2017 Effect of chemical modification of palygorskite and sepiolite by 3-aminopropyltriethoxisilane on adsorption of cationic and anionic dyes. *Applied Clay Science* **135**, 394–404.

Nasrullah, A., Saad, B., Bhat, A. H., Khan, A. S., Danish, M., Isa, M. H. & Naeem, A. 2019 Mangosteen peel waste as a sustainable precursor for high surface area mesoporous activated carbon: characterization and application for methylene blue removal. *Journal of Cleaner Production* **211**, 1190–1200.

Njoku, V. O., Islam, M. A., Asif, M. & Hameed, B. H. 2014 Preparation of mesoporous activated carbon from coconut frond for the adsorption of carbofuran insecticide. *Journal of Analytical and Applied Pyrolysis* **110**, 172–180.

Oyekanmi, A. A., Ahmad, A., Hossain, K. & Rafatullah, M. 2019 Statistical optimization for adsorption of Rhodamine B dye from aqueous solutions. *Journal of Molecular Liquids* **281** (1), 48–58.

Patawat, C., Silakate, K., Chuan-Udom, S., Supanchaiyamat, N., Hunt, A. J. & Ngernyen, Y. 2020 Preparation of activated carbon from *Dipterocarpus alatus* fruit and its application for methylene blue adsorption. *RSC Advances* **10** (36), 21082–21091.

Pereira, V. R., Isloor, A. M., Bhat, U. K., Ismail, A. F., Obaid, A. & Fun, H.-K. 2015 Preparation and performance studies of polysulfone-sulfated nano-titania (S-TiO_2) nanofiltration membranes for dye removal. *RSC Advances* **5**, 53874–53885.

Rafatullah, M., Sulaiman, O., Hashim, R. & Ahmad, A. 2010 Adsorption of methylene blue on low-cost adsorbents: a review. *Journal of Hazardous Materials* **177** (1–3), 70–80.

Rashid, R. A., Jawad, A. H., Ishak, M. A. M. & Kasim, N. N. 2016 KOH-activated carbon developed from biomass waste: adsorption equilibrium, kinetic and thermodynamic studies for Methylene blue uptake. *Desalination and Water Treatment* **57** (56), 27226–27236.

Rashid, R. A., Jawad, A. H., Ishak, M. A. M. & Kasim, N. N. 2018 $FeCl_3$-activated carbon developed from coconut leaves: characterization and application for methylene blue removal. *Sains Malaysiana* **47** (3), 603–610.

Rashid, J., Tehreem, F., Rehman, A. & Kumar, R. 2019 Synthesis using natural functionalization of activated carbon from pumpkin peels for decolourization of aqueous methylene blue. *Science of the Total Environment* **671**, 369–376.

Rashidi, N. A. & Yusup, S. 2017 A review on recent technological advancement in the activated carbon production from oil palm wastes. *Chemical Engineering Journal* **314**, 277–290.

Rattanapan, S., Srikram, J. & Kongsune, P. 2017 Adsorption of methyl orange on coffee grounds activated carbon. *Energy Procedia* **138**, 949–954.

Sahu, S., Pahi, S., Sahu, J. K., Sahu, U. K. & Patel, R. K. 2020 Kendu (*Diospyros melanoxylon Roxb*) fruit peel activated carbon – an efficient bioadsorbent for methylene blue dye: equilibrium, kinetic, and thermodynamic study. *Environmental Science and Pollution Research* **27**, 22579–22592.

Sang, M., Huang, M., Zhang, W., Che, W. & Sun, H. 2019 A pilot bioretention system with commercial activated carbon and river sediment-derived biochar for enhanced nutrient removal from stormwater. *Water Science and Technology* **80** (4), 707–716.

Sangon, S., Hunt, A. J., Attard, T. M., Mengchang, P., Ngernyen, Y. & Supanchaiyamat, N. 2018 Valorisation of waste rice straw for the production of highly effective carbon based adsorbents for dyes removal. *Journal of Cleaner Production* **172**, 1128–1139.

Selvaraju, G. & Bakar, N. K. A. 2017 Production of a new industrially viable green-activated carbon from *Artocarpus integer* fruit processing waste and evaluation of its chemical, morphological and adsorption properties. *Journal of Cleaner Production* **141**, 989–999.

Shahbaz, M., Uddin, G. S., Ur Rehman, I. & Imran, K. 2014 Industrialization, electricity consumption and CO_2 emissions in Bangladesh. *Renewable and Sustainable Energy Reviews* **31**, 575–586.

Sing, K. S. W., Everett, D. H., Haul, R. A. W., Moscou, L., Pieroti, R. A., Rouquerol, J. & Siemieniewska, T. 1985 International Union of Pure and Applied Chemistry: reporting physisorption data for gas/solid systems with special reference to the determination of surface area and porosity. *Pure Applied Chemistry* **57**, 603–619.

Subramani, B. S., Shrihari, S., Manu, B. & Babunarayan, K. S. 2019 Evaluation of pyrolyzed areca husk as a potential adsorbent for the removal of Fe^{2+} ions from aqueous solutions. *Journal of Environmental Management* **246**, 345–354.

Sultana, T., Sultana, S., Nur, H. P. & Khan, M. W. 2018 Characterization of sodium meta-periodate modified betel nut husk fibers reinforced HDPE composites. *European Journal of Advances in Engineering and Technology* **5** (8), 677–682.

Theander, O., Aman, P., Westerlund, E., Andersson, R. & Pettersson, D. 1995 Total dietary fiber determined as neutral sugar residues, uronic acid residues, and Klason lignin (the Uppsala method): collaborative study. *Journal of AOAC International* **78** (4), 1030–1044.

Thommes, M., Kaneko, K., Neimark, A. V., Olivier, J. P., Rodriguez-Reinoso, F., Rouquerol, J. & Sing, K. S. 2015 Physisorption of gases, with special reference to the evaluation of surface area and pore size distribution (IUPAC technical report). *Pure and Applied Chemistry* **87**, 1051–1069.

Tran, T. H., Le, A. H., Pham, T. H., Nguyen, D. T., Chang, S. W., Chung, W. J. & Nguyen, D. D. 2020 Adsorption isotherms and kinetic modeling of methylene blue dye onto a carbonaceous hydrochar adsorbent derived from coffee husk waste. *Science of the Total Environment* **725**, 138325.

Wang, C., Chen, W., Yang, L., Wei, R., Ni, J. & Yang, Y. 2019 Insights into the roles of the morphological carbon structure and ash in the sorption of aromatic compounds to wood-derived biochars. *Science of the Total Environment* **693**, 133455.

Weber, W. J. & Morris, J. C. 1963 Kinetics of adsorption on carbon solution. *Journal of Sanitary Engineering Division* **89** (2), 31–59.

Wekoye, J. N., Wanyonyi, W. C., Wangila, P. T. & Tonui, M. 2020 Kinetic and equilibrium studies of Congo red dye adsorption on cabbage waste powder. *Environmental Chemistry and Ecotoxicology* **2**, 24–31.

Xiao, W., Garba, Z. N., Sun, S., Lawan, I., Wang, L., Lin, M. & Yuan, Z. 2020 Preparation and evaluation of an effective activated carbon from white sugar for the adsorption of rhodamine B dye. *Journal of Cleaner Production* **253**, 119989.

Yu, X., Luo, T., Zhang, Y., Jia, Y., Zhu, B., Fu, X., Liu, J. & Huang, X. 2011 Adsorption of lead(II) on O_2-plasma-oxidized multiwalled carbon nanotubes: thermodynamics, kinetics, and desorption. *ACS Applied Materials and Interfaces* **3** (7), 2585–2593.

Yusriah, L. & Sapuan, S. M. 2018 Properties of betel nut husk reinforced vinyl ester composites. In: *Natural Fibre Reinforced Vinyl Ester and Vinyl Polymer Composites* (S. M. Sapuan, H. Ismail & E. S. Zainudin, eds), Woodhead Publishing, Duxford, United Kingdom, pp. 129–155.

Yusriah, L., Sapuan, S. M., Zainudin, E. S. & Mariatti, M. 2014 Characterization of physical, mechanical, thermal and morphological properties of agro-waste betel nut (Areca catechu) husk fibre. *Journal of Cleaner Production* **72** (1), 174–180.

Zhang, J., Cai, D., Zhang, G., Cai, C., Zhang, C., Qiu, G., Zheng, K. & Wu, Z. 2013 Adsorption of methylene blue from aqueous solution onto multiparous palygorskite modified by ion beam bombardment: effect of contact time, temperature, pH and ionic strength. *Applied Clay Science* **83–84**, 137–143.

Zou, D., Chen, X., Qiu, M., Drioli, E. & Fan, Y. 2018 Flux-enhanced α-alumina tight ultrafiltration membranes for effective treatment of dye/salt wastewater at high temperatures. *Separation and Purification Technology* **215**, 143–154.

Zubrik, A., Matik, M., Hredzák, S., Lovás, M., Danková, Z., Kováčová, M. & Briančin, J. 2017 Preparation of chemically activated carbon from waste biomass by single-stage and two-stage pyrolysis. *Journal of Cleaner Production* **143** (1), 643–653.

First received 29 May 2020; accepted in revised form 3 September 2020. Available online 18 September 2020